Macromolecules

ARTICLE

pubs.acs.org/Macromolecules

Molecular Dynamics Study of Hydrated Poly(ethylene oxide) Chains Grafted on Siloxane Surface

Zuzana Benková,*[,†,‡] Borys Szefczyk,[†,§] and M. Natália D. S. Cordeiro[†]

[†]REQUIMTE, Department of Chemistry, University of Porto, Rua do Campo Alegre 687, 4168-007 Porto, Portugal

[‡]Polymer Institute, Slovak Academy of Sciences, Dúbravská cesta 9, 845 41 Bratislava, Slovakia

[§]Institute of Physical and Theoretical Chemistry, Wroclaw University of Technology, Wybrzeze Wyspianskiego 27, 50-370 Wroclaw, Poland

ABSTRACT: In this work, hydrated poly(ethylene oxide) (PEO) chains composed of varying length N irreversibly grafted to an amorphous siloxane surface by one chain end at different coverage densities σ were studied using atomistic molecular dynamics simulations. We have assessed beginning of the extended overlapping chains (brush regime) at $\sigma = 0.437\ \mathrm{nm}^{-2}$ and identified the mushroom-like conformation of nonoverlapping chains. For the studied systems, the specific interactions lead to density distributions different from the functions analytically derived for model systems. The brush regime demonstrates itself in the density distribution functions and the reduced height h/N evolution with σ. Since the latter dependence indicates $h \sim N\sigma^{1/2}$ scaling, the brush regime corresponds to the situation of a concentrated aqueous PEO solution with a correlation length $\sigma^{-1/2}$. The extrapolated thickness of PEO brushes reproduces experimental results fairly well. Water molecules prevent EO monomers from an adsorption to the siloxane surface.

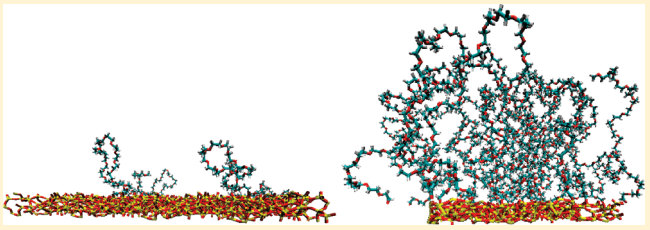

1. INTRODUCTION

In recent years, a great deal of attention at both theoretical and experimental level has been paid to polymeric brushes because of their important biological and technological properties, which in turn are utilized in, e.g., lubrication,[1] colloid stabilization,[2] or inhibition of deposition on surfaces.[3,4] The polymeric brushes are formed of polymer chains densely attached at one of their ends to a solid surface or an interface, reversibly by physical adsorption or irreversibly by covalent chemical bonds. The case in which chains are attached chemically is much more easily comprehended by theoretical approaches and is relevant to many practical applications such as biocompatibility and surface modified liposomes.[5,6] The brush regime might be achieved if the coverage surface density (the inverse substrate surface area occupied by one chain) exceeds $\sim 1/(\pi R_g^2)$, where R_g is the radius of gyration of a corresponding free chain. Below this coverage density the chains are not overlapped and, when grafted on a nonadsorbing surface, constitute an array of "mushrooms" of dimensions comparable to their free chain dimensions. For chains of intermediate lengths the transition between both regimes is not step-like and many experimental studies have been performed on systems belonging to this transition region.[7,8]

The properties of polymer brushes can be tuned by manipulating the number of segments and molecular architectures of the grafted polymer chains, the coverage densities of modified surfaces, the interactions of monomers with surface, the temperature and the solvent quality.

In the brush regime, due to the lateral repulsion, the chains expand in the direction perpendicular to a surface until the loss of entropy caused by the reduced degrees of freedom in stretched entities as well as spatial confinement is counterbalanced by the gain of negative enthalpy from reducing the excluded volume interactions between chains. The height of a brush layer h depends on the coverage density σ, the length of grafted chains N and the solvent quality.

The scaling approach of Alexander[9] and the Flory-type arguments of de Gennes[10] both show that the height of a brush under good-solvent conditions scales as $h \sim N\sigma^{1/3}$. This linear relation of the chain height to its contour length N means more significant stretching when compared with the extension of a free chain induced by the good solvent and scaling as $\sim N^{3/5}$. Regarding the analytical self-consistent-field (SCF) theory[11−13] for polymer brushes built by structureless chains, it is formulated with the assumption that the excluded volume interactions are relatively weak. Thus, it assumes that the coverage density is high enough for the applicability of Gaussian statistics or, in other words, the size of the thermal blobs should be larger than the distance between grafting points, but at the same time, it should be not too high to allow for truncation of the three-body interactions. The outcome of the SCF analysis is in qualitative agreement with the former predictions for the brush height and differs only in a numerical prefactor. While, according to Alexander[9] and de Gennes,[10] the density distribution of chain monomers in the direction perpendicular to the grafting plane is a step function steeply decaying to zero at the brush height, SCF theory provides the parabolic monomer-density dependence on the distance from the grafting surface which

Received: February 1, 2011
Revised: March 16, 2011
Published: April 01, 2011

vanishes at the brush height. Using the SCF approach, Milner et al.[11−13] also showed that the free ends of grafted polymers have nonzero probability of distribution everywhere in the brush with a linear initial increase, faster decay after maximum at $h/2^{1/2}$ and zero value at h. On the opposite, the scaling approach assumes that the free chain ends of a brush are strictly located at the frontal edge of the brush layer.[9,10]

Besides the above-mentioned limitations, the SCF analysis considers also very long chains. Nevertheless, for many biological applications, the polymers used to form brushes are of relatively low molecular weight (less than a few hundred segments) and the modified systems do not necessarily meet the criteria for the reliability of the SCF results. For the description of brushes based on intermediate-chain lengths, alternative methods like the numerical SCF approach[14,15] or the single-chain mean-field theory[16,17] can be used.

Along with experimental techniques such as surface force apparatus,[18] small angle neutron scattering[19] and neutron reflectivity,[20] the molecular computer simulations including molecular dynamics (MD),[21−23] Monte Carlo (MC),[24−27] dissipative particle dynamics (DPD),[28] and Brownian dynamics (BD)[29] play an important role in the elucidation of polymeric brush structures. However, most of the computer simulations are carried out using predominantly the coarse-grained representation for polymer chains tethered to an unspecific surface with solvent conditions modeled implicitly, whereas atomistic studies using MD[30,31] or MC[32,33] simulations are rather scarce.

Poly(ethylene oxide) (PEO) terminated by OCH_3 (methoxy) group or poly(ethylene glycol) (PEG) terminated by OH (hydroxyl) group built up of $O-CH_2-CH_2$ monomers belong to the simplest synthetic polymers from the viewpoint of chemical composition. Because of their amphiphilic nature, good solubility in water and organic solvents, biocompatibility, nontoxicity and low immunogenicity, these polymers are most frequently encountered in biomedical and biotechnical devices. Surface fabrication of drug delivery systems with PEO enhances the solubility of hydrophobic drugs, prolongs circulation time, minimizes nonspecific interactions, improves specific targeting to, and fusion with a cell. Of special relevance is the protein-resistance of surfaces modified by PEO polymeric chains which is successfully used in medicine to reduce protein adsorption on the surfaces.[34,35] The protective efficiency of the coated surfaces depends on the thickness of the grafted layers and their surface coverage.

Rather peculiar is the exceptional water solubility of PEO chains for a very wide range of polymerization degrees and practically in all proportions. In contrast to normal polymer behavior, at elevated temperatures, PEO-water miscibility declines and above the critical temperature phase separation occurs. At even higher temperatures, the homogeneous PEO-water system is regained.[36] Such a closed loop phase diagram is typical for polymers forming hydrogen bonds with their solvating medium. However, closely related polyethers do not exhibit complete solubility in water at room temperature. In the case of PEO, the perfect solubility in water is ascribed to the ability of PEO chains to adopt conformations with oxygen atoms fitting into the tetrahedral-water-lattice points.[37]

Despite the frequent application of PEO in drug delivery system carriers, just to mention one example, the effect of the molecular weight and coverage density on physical properties has still not been elucidated completely. Here, we present molecular dynamics simulations of relatively short PEO chains chemically grafted on amorphous silica in water as a model for the systems based on surfaces coated by PEO layers. In practice the molecular weight of PEO chains used to modify the surfaces is often about 2000 $g\cdot mol^{-1}$ (∼45 monomers) which is below the critical molecular weight of entanglement for PEO chains in melt estimated between 3200 and 4400 $g\cdot mol^{-1}$;[38] for instance, experimentally grafted chains as short as 3−15 EO monomers have been studied.[8] In the present work, we focus on the conformation and thickness of PEO layers as a function of the chain length and coverage density.

The calculations should shade light on the character of transition from the mushroom- or pancake-like regime to the brush regime and approximately locate the onset to the brush regime. We have investigated the monomer density distributions, the distributions of the free terminal monomers and individual monomers along the chain as functions of the distance from the siloxane surface and we have located the mushroom-brush transition. The situation in the brush regime for hydrated PEO brushes corresponds to the concentrated solutions.

The rest of this paper is organized as follows: section 2 presents details of the MD simulations and the description of system; section 3 deals with the results, and our main conclusions are summarized in section 4.

2. METHODOLOGY

The systems composed of PEO chains attached to an amorphous siloxane substrate (silica without free OH groups) at one end, terminated by methyl group at the other end and submersed in water were simulated using MD method. PEO chains comprised N = 18, 24, 30 oxygen atoms with the last one harmonically bonded to a silicon atom. The symbol N identifies the number of monomers throughout the paper. The coverage densities of grafted PEO chains, expressed as the number of chains attached to a unit area, were σ = 0.055, 0.109, 0.218, 0.437, 0.874, and 1.092 nm^{-2}. The starting conformations of the systems were constructed as stretched, rod-like PEO chains with the helical axis vertically oriented to the siloxane plane and immersed in water. Atoms of the amorphous siloxane surface were kept frozen during the MD simulations and participated only in nonbonded interactions with the atoms of PEO chains and water. All MD simulations were performed using the GROMACS package.[39,40] The all-atom intra- and intermolecular interactions were described by the revised CHARMM force field[41,42] and the TIP3P model[43,44] for water molecules. In the case of Lennard-Jones interactions for molecules of water, only oxygen atoms were assumed as interaction sites, even though the CHARMM force field in combination with the TIP3P model originally considers extended TIP3P model with interacting hydrogen atoms as well. However, as it has been shown, such a simplification does not deteriorate the results and significantly speeds up the calculations when exploiting the highly efficient inner loop for nonbonded interactions, which involve water molecules as implemented in GROMACS.[45] The Lennard-Jones parameters used for silicon and oxygen atoms within the siloxane layer were compatible with the CHARMM force field and TIP3P water model.[46] Since the periodic boundary conditions were applied in all dimensions, the heights as well as the sides of square based simulation boxes were set sufficiently long to prevent the interactions between a given particle and its periodic image in all directions. Although this study is devoted to structural properties we have preferred MD over MC approach because of the effective algorithms implemented in the GROMACS software along with its convenient parallelization, and because in the future simulations we intend to study structural and dynamic properties of water molecules at the water-bare and at the water-PEO modified siloxane interfaces.[47]

First the systems were simulated at semi-isotropic NPT conditions (P = 1 bar, T = 298 K) for 100 ps using Parrinello-Rahman barostat[48,49] with a relaxation time of 0.5 ps. During this stage of the simulation, all bonded parameters were fully unconstrained and the time step was set to 1 fs. The final conformations from these constant surface pressure runs were then

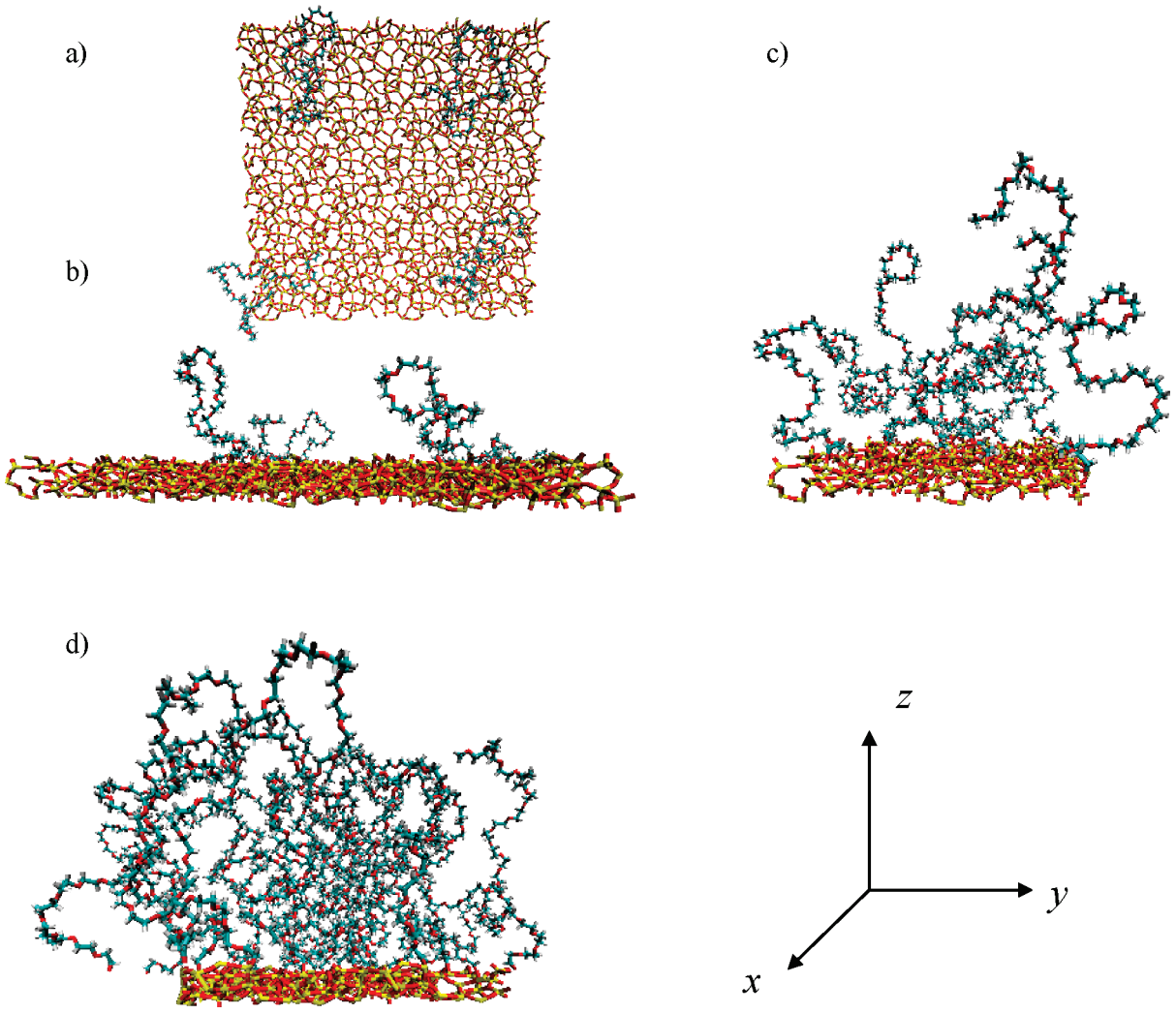

Figure 1. Snapshots displaying a top view (a) and side views (b−d) of PEO chains of length $N = 30$ grafted on the siloxane surface. Water molecules are removed for the sake of clarity and the Cartesian framework depicts the orientation of the systems in the simulation boxes. The coverage densities are (a, b) 0.055 nm^{-2}, (c) 0.437 nm^{-2}, and (d) 1.092 nm^{-2}.

used as input structures for *NVT* ensemble simulations with all bond lengths constrained by the LINCS algorithm[50] and with a time step of 2 fs. The temperature was kept fixed at 298 K by Nosé-Hoover thermostat[51,52] and resorting to a relaxation time of 0.1 ps. After an equilibration period of 10 ns, averaging was carried out over all chains on a trajectory length of 20 ns. The time interval between sampling conformations was 5 ps. The relaxation times extracted from the autocorrelation functions of the end-to-end distance and radius of gyration for the grafted PEO chains in aqueous solution were in all studied systems less than 2 ns. The long-range electrostatic interactions were treated with the particle-mesh Ewald method[53,54] with the real space cutoff set to 1.4 nm. The Lennard-Jones (L-J) potential was smoothly shifted to zero between 1.0 and 1.2 nm. Both, the real-space part of the Ewald summation and the short-range L-J interactions, were calculated within a radius of 1.4 nm with help of a neighbor list updated every 10 time steps.

3. RESULTS AND DISCUSSION

3.1. Monomer Density Distributions. Figure 1 displays snapshots of PEO chains composed of 30 monomers attached to the siloxane. For better clarity the water molecules are omitted in these representations and the Cartesian coordinate system illustrates the orientation of the systems in the simulation boxes. As it is evident, the chains in the system with the lowest coverage density are completely isolated. The partial overlap is induced for this chain length ($N = 30$) at the coverage density of 0.109 nm^{-2} while, for the shorter chains ($N = 18$ and 24), a similar conformation is observed at the coverage density of 0.218 nm^{-2}. The isolated conformations of the chains, their extended arrangement, vertical to the siloxane surface, and the transition between these two limiting structures in the water environment are well detectable in the 3D radial distribution functions of the PEO backbone atoms presented in the scaled form (Figure 2). Multiplying the radial distribution function by the coverage density removes its dependence on the coverage density. As can be seen in Figure 2, the plots of the two most densely attached chains appear almost collapsed and the systems of the two lowest coverage densities are distinguished in a similar way. The regime of dense arrangement is separated out by the intermediate coverage densities which constitute the transition region. All plots for grafted chains are akin to the plot for a free PEO with four characteristic peaks of declining amplitudes with the increasing radius. The first peak is predominantly due to the

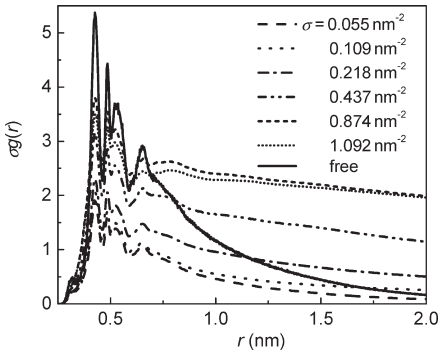

Figure 2. Scaled 3D radial distribution functions of the backbone atoms for PEO chains of length $N = 30$ grafted at different coverage densities σ. The radial distribution function for a free chain was divided by 25 for the sake of better comparison.

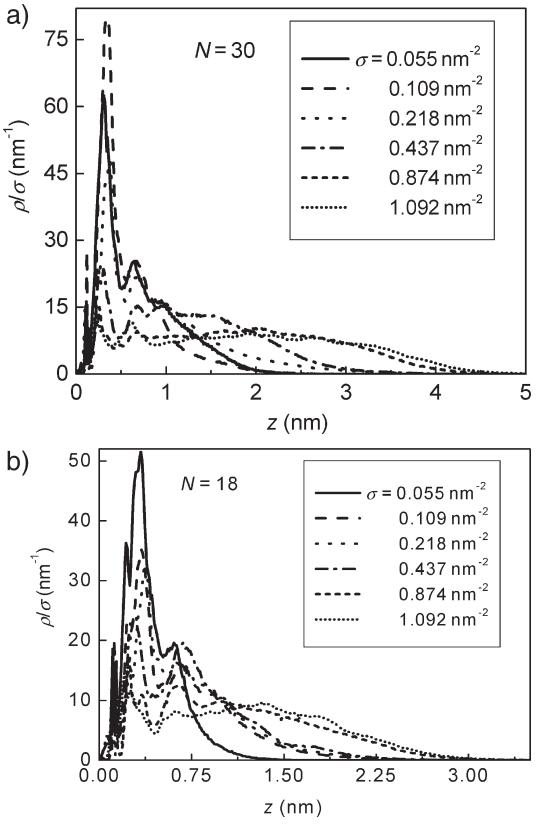

Figure 3. Monomer density distribution reduced by the respective coverage density as a function of the distance from the siloxane surface for PEO chains of (a) $N = 30$ and (b) $N = 18$ grafted at different coverage densities σ.

oxygen−carbon interaction with a minor contribution of carbon−carbon interaction while the second peak is due purely to the carbon−carbon pair. Some preferential organization of chain fragments near the siloxane surface is evident from the unsymmetrical plot of dihedral distributions (data not shown). Since the underlying surface is of amorphous nature such an arrangement can be triggered by the atomic structure of the aqueous environment and the solid surface has only nonspecific anchoring function. Monomeric fragments far away are less locked and rotate more freely.

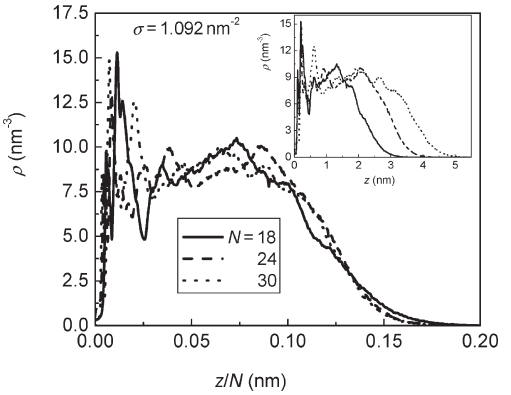

Figure 4. Monomer density distribution as a function of the distance from the siloxane surface reduced by the number of monomers for layers built up of PEO chains of $N = 18$, 24, and 30 grafted at coverage density $\sigma = 1.092$ nm^{-2}. The inset shows the same variation with the distance from the surface.

The monomer density distribution ρ reduced by the coverage density σ as a function of the distance from the siloxane surface for chains of length $N = 30$ grafted at the different coverage densities (Figure 3a) displays a rich structuring in the close proximity of the siloxane layer consistently with other molecular simulation studies.[21−23,28] Similarly to other atomistic simulations,[30,31] the density profile is not parabolic, with a maximum at $z = 0$ as proposed by the self-consistent-field theory. After the initial oscillations the density distribution vanishes either immediately, in the case of the three lower coverage densities or, in the case of the higher coverage densities, after a plateau with its width correlating with the coverage density. The first very narrow peak is found about 0.1 nm apart from the siloxane surface, and reflects the location of the first carbon atom attached to the oxygen atom of the PEO chain, which is assumed to be fixed within the siloxane surface in the simulations. The relatively largest normalized intensity ρ/σ of the second peak, formed from contributions of oxygen and carbon atoms and positioned between 0.25 and 0.33 nm, possesses strong sensitivity to the coverage density. For the most densely grafted chains, this peak displays only marginal intensity. The third layer of relatively low amplitude is observed at a distance slightly above 0.65 nm from the siloxane surface. The magnified amplitudes of the reduced density of the second and third peak found for the two smallest coverage densities indicate the capacity of the space near the siloxane surface to accommodate the EO monomers along the chain backbone. The pattern of the layers near the solid surface turns out to be the same also for the tethered layers comprising 18 (Figure 3b) and 24 monomers but the flat region following the oscillations is considerably shrunk and the third peak almost disappears for the largest coverage densities in the two latter cases. At this point it should be mentioned that the positions of the first three peaks of hydrated brushes in the monomer distribution functions match their dry analogues,[55] thus the water does not affect the monomer layering near the solid surface and just damps the amplitudes. The fourth and fifth peaks present in dry systems vanish in water medium.

According to the SCF theory the density distribution of chain segments tethered to a solid surface may be expressed by a scaling form as

$$\frac{\rho(z)}{\sigma^{2/3}} = f\left(\frac{z}{N\sigma^{1/3}}\right) \quad (1)$$

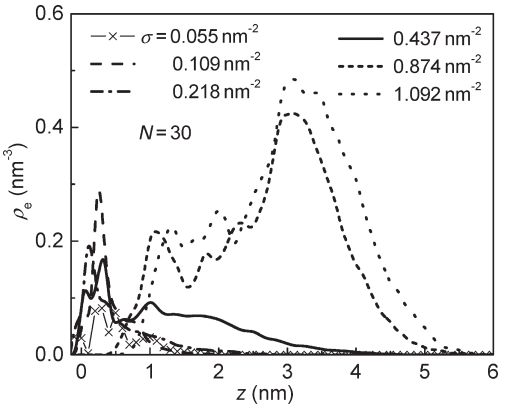

Figure 5. Density distribution of the free terminal PEO atoms as a function of their distance from the siloxane surface for PEO chains of $N = 30$ grafted at different coverage densities σ.

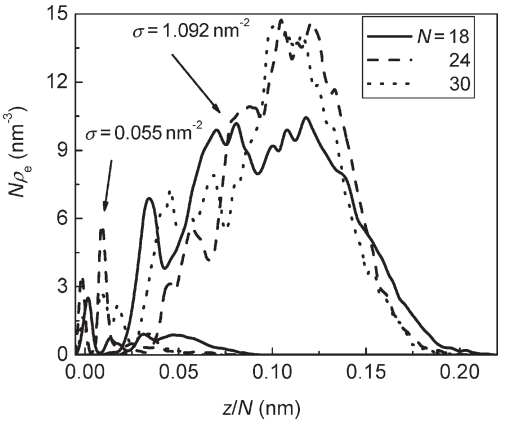

Figure 6. Scaled density distribution of the free terminal PEO atoms as a function of their scaled distance from the siloxane surface for PEO chains of N monomers grafted at indicated coverage densities σ.

This implies that, at a constant coverage density σ, the plot of monomer density distribution ρ vs the distance of monomers from the solid surface z reduced by the chain length N for different N's should collapse into one single curve. Figure 4 illustrates such a plot for the highest coverage density. We have examined if such coalescence occurs in the flat region of the density distribution for the PEO layers of the highest coverage densities where the plateau is well developed. As shown in Figure 4, the curves are getting closer upon reduction of z abscissa but an acceptable collapse occurs only in the tailing region. This, along with the shape of the density distribution curve which is inconsistent with the one suggested by the SCF theory, is not surprising since the presented systems are built of short polymeric chains specifically interacting with the solvent environment and solid substrate.

3.2. Density Distribution of Free Chain Ends. Figure 5 depicts the probability ρ_e to find the free ends of PEO chains composed of 30 monomers at the distance z from the grafting surface. The terminal atoms of PEO chains tethered at the lowest coverage densities $\sigma = 0.055, 0.109, 0.218$ nm^{-2} are not excluded from the immediate contact with the siloxane. Since the free terminal monomers are not restricted substantially by the inner monomers they have the freedom to move similarly to the remainder of the chain and the distribution functions of the free ends are qualitatively reminiscent of the corresponding monomer density distributions (Figure 3a), i.e., gradually damping intensities of peaks further from the siloxane surface. For the shorter chain lengths this similarity remains also at higher coverage densities. The depletion zone in the region close to the solid surface is observed only for the two highest coverage densities.

According to the SCF theory, the formula for the distribution function of the free chain ends has the following functional form

$$\frac{\rho_e(z)N}{\sigma^{2/3}} = f\left(\frac{z}{N\sigma^{1/3}}\right) \qquad (2)$$

This has prompted us to plot the scaled distribution $N\rho_e$ vs reduced coordinate z/N at fixed coverage density for chains of different lengths to examine the qualitative behavior of this function for the presented realistic systems composed of relatively short chains. This plot for PEO chains grafted at $\sigma = 0.055$ and 1.092 nm^{-2} is presented in Figure 6. Similarly to the scaled plot of ρ vs z/N one can hardly anticipate perfect quantitative

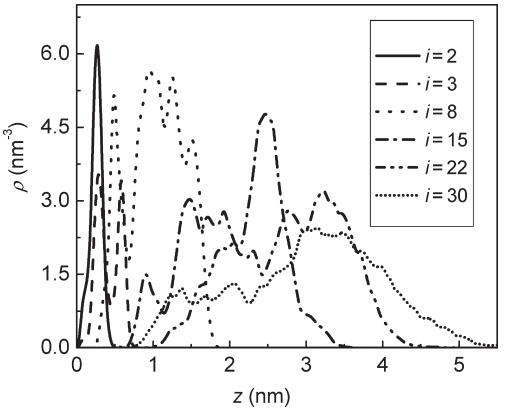

Figure 7. Density distribution of $O-CH_2^*-CH_2$ monomers (the asterisk assigns the reference atom) as a function of the distance from the siloxane surface for the ith monomer of PEO chains composed of $N = 30$ monomers grafted at the coverage density $\sigma = 1.092$ nm^{-2}. Index i is measured from the grafting point onward. The densities for $i \geq 8$ are multiplied by 5 for the sake of better comparison.

agreement between the investigated real systems with the model systems subject to the restrictions imposed by the SCF analysis. However, comparison of Figure 6 (the chain end distribution) with the analogous plot for the monomer distribution in Figure 3 reveals that the qualitative behavior is even worse.

3.3. Density Distribution of Individual Monomers and Their Distance from Siloxane Surface. Useful information on grafted chain conformations can be extracted from the density distribution function of individual monomers. Such distribution functions for some selected segments i, indexing from the grafting surface onward within the chain backbone of $N = 30$ grafted at coverage density $\sigma = 1.092$ nm^{-2}, are displayed in Figure 7. Remarkably, the distributions are not strictly monomodal in contrast to the simulations employing the bond fluctuation model on a lattice.[25] The distributions of monomers with $i > 15$ exhibit pattern similar to the distribution of the terminal atom with broad maxima shifted further from the siloxane surface as i increases. A similar trend is found also for monomers with $i < 15$. The distributions are getting broader as the index increases which is expected due to the less restricted space available for the movement of monomers more distant

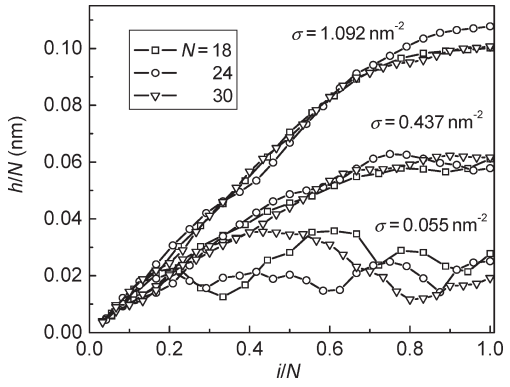

Figure 8. Reduced average distance of the i-th monomer from the siloxane surface versus the reduced contour position of the ith monomer for PEO chains of lengths N grafted at indicated coverage densities σ.

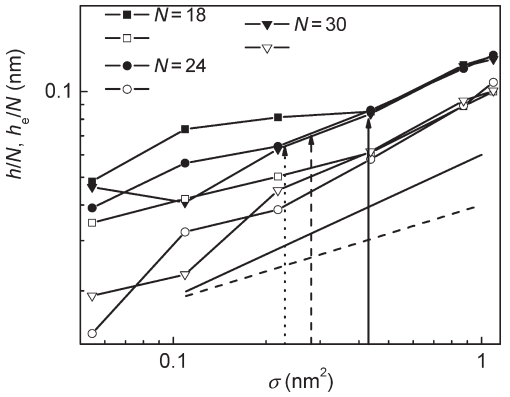

Figure 9. Average height of the PEO layer (solid symbols) and the average distance of the terminal backbone atoms from the siloxane surface (open symbols) reduced by the number of monomers plotted against the coverage density for grafted chains of contour length N in the logarithmic scale. Solid, dashed, and dotted arrows indicate the values $1/(\pi R_g^2)$, the estimated mushroom-brush crossover, for $N = 18$, 24, and 30, respectively, with R_g being the free chain radius of gyration. The full and dashed lines with the slopes of 1/2 and 1/3, respectively, are also displayed for comparison.

from the solid surface. This has also been found in another simulation study on model anchored chains.[25] A pronounced bimodality of the probability distribution of two narrow peaks is observed for monomer with $i = 3$. The bimodality of the distributions although, less sharp with increasing i, is observed also for more sparsely attached as well as shorter chains and is characteristic for monomers whose distributions virtually vanish after $z \approx 1.5$ nm. This region above the siloxane surface is more populated by monomers (Figure 3a,b). Consequently, because of the lateral crowding, monomers prefer oscillating motion in directions vertical to the siloxane surface. We have monitored these discrete jumps by visualizing the trajectory of the respective monomers and they manifest themselves by two peaks in distribution functions of isolated monomers.

As regards the average distances from the siloxane surface $h(i)$ for the consecutive monomers i in chain backbone, these have been evaluated as the normalized first moment of the respective monomer density distribution, i.e., as

$$h(i) = \int_0^\infty z\rho_i(z)\,\mathrm{d}z \Big/ \int_0^\infty \rho_i(z)\,\mathrm{d}z \qquad (3)$$

These distances reduced by the number of monomers N are plotted against the reduced monomer index i/N in Figure 8 for PEO chains of all investigated chain lengths grafted at the coverage densities $\sigma = 0.055$, 0.437, and 1.092 nm^{-2}. The $h(i)$ curve is monotonous, steeper and saturates for $i/N > 0.7$ for densely attached chains; this shape is similar to the one reported for on-lattice model systems.[25] The linear relation between the monomer distance from the solid surface and the chain contour length is apparent from the collapsing tendency of the reduced plots for different lengths of PEO chains in the brush regime. For the sparsely grafted PEO chains an oscillating trend instead of the linear evolution is achieved already near the siloxane surface. In the nonoverlapping regimes the lower is the coverage density the more space the monomers have to remain more or less near the siloxane surface (as shown by the oscillations). They are also not forced to stretch away from the surface as in the case of denser grafting.

3.4. Extension of PEO Chains and Characterization of the Brush Regime. *3.4.1. Height and Free-Chain-End Distance of PEO Layers from Siloxane Surface and Mean-Square End-to-End Distance of PEO Chains.* The variation of the dimensions for PEO chains attached to the siloxane surface at the lowest coverage densities with the chain contour length N is governed by a scaling relation with scaling exponent smaller than 3/4 derived for a free two-dimensional coil in a good solvent.[56] This implies that nonoverlapping PEO chains end-grafted onto the siloxane surface are not strongly adsorbed by the siloxane layer and adopt curly three-dimensional mushroom-like conformations instead of pancake-like ones as is recorded also in Figure 1, parts a and b.

The thickness of the brush layer under the given experimental conditions is the most relevant characterization of brush systems easily available at the experimental level (exploiting, e.g., ellipsometry, X-ray photoelectron spectroscopy or atomic force microscopy) and tunable by the molecular weight of grafted polymers and by the coverage density. The average thickness or height h of the investigated systems was computed as the doubled normalized first moment of the monomer density distribution function:

$$h = 2\int_0^\infty z\rho(z)\,\mathrm{d}z \Big/ \int_0^\infty \rho(z)\,\mathrm{d}z \qquad (4)$$

This quantity has a well-defined dependence on the chain length and coverage density for good-solvent, Θ-solvent (with ideal-chain statistics) and poor-solvent conditions, at which a simple scaling analysis yields $\sim N\sigma^{(1-\upsilon)/2\upsilon}$ with exponents $\upsilon = 3/5$, 1/2, and 1/3, respectively. Notable is the linear dependence on the contour chain length, regardless of the solvent quality. The average distance of the free chain ends h_e from the siloxane surface was also computed from eq 3 using the probability distribution of the terminal segments ρ_e. The height of the PEO layer and the average distance of the chain end from the siloxane surface reduced by the number of segments N are plotted as functions of the coverage densities in the logarithmic scale in Figure 9 for all studied chain lengths. As can be seen in Figure 9, the plots for both properties start overlapping at the coverage density 0.437 nm^{-2}. At the experimental level, the brush regime has been reported even for the shorter PEO chain length comprising 12 monomers grafted on a lipid monolayer supported by a hydrophilic silicon oxide,[8] although the SCF and scaling theories assume $N \gg 1$. The arrows in Figure 9 correspond to $1/(\pi R_g^2)$ (R_g is the average radius of gyration of free

dx.doi.org/10.1021/ma200233g |*Macromolecules* 2011, 44, 3639–3648

chains in water) and roughly identify the expected onset of the brush regime.

Based in Figure 9 we may clearly distinguish the brush regime at $\sigma \geq 0.437$ nm^{-2}, for all chain lengths. From this point on the linear dependences $h \sim N$ and $h_e \sim N$ hold for all three chain lengths and the line in the logarithmic scale indicates scaling behavior as established by the theoretical analysis. Nevertheless, instead of the exponent equal to 1/3 as expected for PEO brushes in water which is a good solvent for PEO chains,[57] the obtained exponent (0.49) is higher and approaches 1/2 as derived for the Θ solvent. The best linear fit to the dependence of the average height and free-chain-end distance from the siloxane surface on the variable parameter $N\sigma^{1/2}$ displayed in Figure 10 supports the findings shown in Figure 9. This observation means a contraction for $\sigma < 1$ and an expansion for $\sigma > 1$ when compared to the $\sigma^{1/3}$ dependence and may be interesting from an experimental point of view.

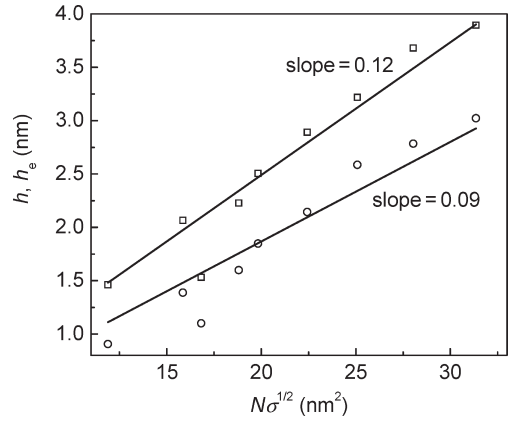

Figure 10. Average height (squares) and average distance of the free chain ends from the siloxane surface (circles) as a function of the variable $N\sigma^{1/2}$ for PEO brushes composed of N = 18, 24, and 30 monomers grafted at the coverage densities σ = 0.437, 0.874, and 1.092 nm^{-2}. Solid lines denote the best linear fits with the values of slopes provided.

Table 1 contains the mean-square end-to-end distance $\langle R^2 \rangle$, its mean-square z component $\langle R_z^2 \rangle$, average height of the brush h and average distance of the free chain ends from the siloxane surface h_e for all simulated chain lengths of PEO chains grafted at the coverage densities conforming to the brush regime. One should remark here, in the context of the standard deviation, that the variation in the coverage densities has been realized by the variation of the number of chains at a constant surface area. In this way the statistics are improved for larger coverage densities (more chains). This should be kept in mind when comparing the standard deviations between different coverage densities. In the brush regime, the extension of chains away from the grafting plane is reflected on the magnitude of the z component of the end-to-end distance which exceeds the corresponding magnitude for free chains of the same contour length (Table 1), as expected due to the lateral crowding effect. The ratio $\langle R^2 \rangle / \langle R_z^2 \rangle$ for PEO chain brushes is lower than the ratio for free chains as well as lower than 3, the estimate for a perfect spherical coil apart from the brush of PEO chains with 18 monomers grafted at 0.437 nm^{-2}. Most likely, the latter irregularity is due to the fact that this system is approximately at the mushroom-brush transition. Free chains possess values of $\langle R^2 \rangle / \langle R_z^2 \rangle$ also slightly different from 3, which is consistent with the ellipsoidal rather than spherical shape of polymer coils.[58] Most densely tethered chains are expanded up to almost 40% of their totally straightened rod-like conformation.

3.4.2. Scaling of Height and Free-Chain-End Distance of PEO Brushes from the Siloxane Surface. In what follows we rationalize the ideal scaling of the height and of the free-chain-end distance of PEO brushes from the siloxane surface found in the present simulations and discussed in the previous subsection in terms of a transition length scale. For these purposes, it is useful to introduce a transition length scale, termed as the

Table 1. Mean-Square End-to-End Distance $\langle R^2 \rangle$, Its Mean-Square z Component $\langle R_z^2 \rangle$ with Standard Deviations, Average Height of the Brush h and Average Distance of the Free Chain Ends h_e from the Siloxane Surface for PEO Chains of N Monomers Grafted at Coverage Densities σ[a]

σ (nm^{-2})	$\langle R^2 \rangle$ (nm^2)	$\sigma(R^2)$ (nm^2)	$\langle R_z^2 \rangle$ (nm^2)	$\sigma(R_z^2)$ (nm^2)	$\langle R^2 \rangle / \langle R_z^2 \rangle$	h (nm)	h_e (nm)	L (nm)
				N = 18				
0.437	4.98	2.21	1.44	1.50	3.47	1.53	1.10	
0.874	5.19	2.66	2.83	2.41	1.83	2.23	1.60	
1.092	5.26	2.92	3.32	2.43	1.58	2.40	1.80	
free	4.39	2.69	1.42	1.60	3.08			6.34
				N = 24				
0.437	4.83	2.45	2.02	1.82	2.39	2.07	1.39	
0.874	6.80	3.85	4.77	3.73	1.42	2.89	2.14	
1.092	8.73	3.90	6.62	3.49	1.32	3.22	2.59	
free	7.04	4.95	2.45	3.15	2.88			8.50
				N = 30				
0.437	7.11	3.27	3.88	3.46	1.83	2.51	1.85	
0.874	10.38	5.55	7.99	5.09	1.30	3.68	2.78	
1.092	11.25	5.78	9.24	5.33	1.22	3.89	3.02	
free	8.58	6.01	3.30	4.02	2.60			10.66

[a] For comparative purposes, mean-square end-to-end distance and its mean-square z component for free PEO chains as well as the length of an entirely straightened backbone L, are also included.

thermal blob size ξ_T.[56] This size of a semiflexible chain is governed by the excluded volume defined as:

$$v = (1 - 2\chi) l_P{}^2 a \quad (5)$$

where the monomer size a = 0.36 nm, assessed from the radial distribution function, and in our case is close to the experimental results 0.35 nm.[59] Our persistence length l_P = 0.39 nm, which expresses a measure of the chain stiffness and has been evaluated from the end-to-end distance relation established for the worm-like chain model, is slightly above the experimental value of 0.37 nm.[60] Note that the ratio $l_P/a \approx 1$ indicates a rather flexible character of the PEO chains. The Flory interaction parameter χ bears information on the solvent quality. For PEO−water systems this parameter is not only temperature dependent but also depends on the concentration and molecular weight of PEO.[61] The quality of the solvent is dictated by the excluded volume, in particular, if $v > 0$, the solvent is good for a given polymer, if $v \approx 0$, a polymer is in a Θ solvent, and if $v < 0$, the solvent is poor. In a good solvent, the excluded volume interactions between monomers of the same chain are relevant only if the number of monomers in the chain exceeds certain value g_T. On the length scale which contains g_T monomers and which is termed as the thermal blob ξ_T the monomers obey statistics of an ideal chain. Thus, the following relation between the thermal blob size ξ_T and the number of monomers g_T holds:

$$\xi_T = (2 a l_P g_T)^{1/2} \quad (6)$$

The number of monomers within a thermal blob can be estimated from the chain interaction parameter z defined as[56]

$$z = \left(\frac{3}{2\pi}\right)^{3/2} \frac{v}{a^3} N^{1/2} \quad (7)$$

which must satisfy $z > 1$ for excluded volume interactions to be observed under good-solvent conditions, otherwise monomers within the same free chain do not interact with each other and such a chain behaves like an ideal one. If $z \approx 1$ the chain length just stands for one thermal blob which means $N = g_T$. If this condition is applied to eq 7, by substituting v with eq 5 and N with eq 6, the size of a thermal blob reads

$$\xi_T = \left(\frac{2\pi}{3}\right)^{3/2} \left(\frac{a}{l_P}\right)^2 \frac{(2 a l_P)^{1/2}}{(1 - 2\chi)} \quad (8)$$

In addition, in the brush regime a new correlation length $\xi = \sigma^{-1/2}$ appears, defining the size of a blob. Within the blob concept, the ideal-chain statistics applies provided $\xi_T > \xi$.[62] The chain in a brush is then represented by a linear array of blobs of dimension ξ with the ideal statistics of segments inside each blob. The lowest limit of the thermal blob size ξ_T for an athermal solvent (in which case $\chi = 0$ and thus, $v = l_P{}^2 a$) is 1.37 nm for PEO chains, assuming monomer size and persistence length as calculated for the aqueous solvent in the present MD simulations. Even this lowest possible value of the thermal blob size is sufficiently large for the ideal behavior of PEO chains in brushes of σ = 0.874 and 1.092 nm^{-2} with respective ξ = 1.07 and 0.96 nm. If $\chi > 0.05$ one may expect an ideal statistics at all coverage densities satisfying the brush regime conditions. However, the Flory interaction parameter for PEO-water systems may reach values above 0.4[61,63] which gives ξ_T = 6.8 nm.

For instance, the experimental works report significant coverage densities of PEO brushes as high as 3.4 nm^{-2} for chains of about 2000 g·mol^{-1}.[64] The upper limit for the coverage densities is limited by the mass density of PEO chains in their melt. The correlation sizes ξ for these coverage densities are rather small and are highly probable to diminish below the thermal blob size ξ_T with consequent ideal behavior of grafted chains on all length scales. The situation in brushes, with the characteristic correlation length determined by the coverage density, implies an ideal (Gaussian) statistics in concentrated solutions. Moreover, the molecular weight of ≈2000 g·mol^{-1}, commonly used in experiments on PEO-coated surfaces is hardly enough to create more than two thermal blobs even of a free chain. This implies that the brush conformations are governed by the ideal statistics for all coverage densities since this is the dominant statistics for a free PEO chain.

3.4.3. Comparison with Experiments and Other Molecular Simulations. Thickness of PEO brushes assessed from the ellipsometric measurements in water at 20 °C was 2.8 ± 0.1 nm for chains of molecular weight 526 g·mol^{-1} (12 EO monomers) grafted at 2.3 ± 0.1 nm^{-2}, and 7.5 ± 0.3 nm for chains of molecular weight 2000 g·mol^{-1} (45 EO monomers) grafted at 1.0 ± 0.1 nm^{-2}.[59] Our results extrapolated using the function h vs $N\sigma^{1/2}$ for the brush regime outlined in Figure 10 give thicknesses of 2.2 and 5.9 nm for N = 12 and 45, respectively. These values satisfactorily compare with the experimental results. Although, our MD simulations have been performed at a slightly different temperature (25 °C), for such short chains, and at such temperatures the effect should be negligible, and if anything happens, the chains should shrink.[36] More contribution to the measured thickness is expected from the methacrylic spacer through which the bonding of PEO polymers was realized at the experimental level.

The highest coverage density 1.092 nm^{-2} used in the present MD simulations of PEO brushes conforms to the average-mass density of about 0.6 g·cm^{-3} in the region of brush layer evaluated as $\sigma M_N/hN_A$, being M_N the molar mass of a PEO chain of a particular length N and N_A the Avogadro's number. This value is about half of the density of the PEO melt and is between the experimental average-mass densities of hydrated layers of PEO brushes assessed to be around 0.73 g·cm^{-3} for N = 12 monomers and 0.44 g.cm^{-3} for N = 45 monomers.[64] The latter figures were extracted from $\rho_{melt} h_{dry}/h_{hyd}$ (ρ_{melt} is the density of PEO melt and h_{dry} and h_{hyd} are the heights of dry and hydrated PEO brushes, respectively). Comparisons with other experiments are often complicated because of the spacers or lipid (lipopolymeric) layers such as a frequently used distearoylphosphatidyl ethanolamine (DSPE) through which the PEO polymers are deposited on glass surfaces. Furthermore, different experimental techniques do not render unified thickness of PEO layers and usually, quite big uncertainties have been observed.[65,66]

We have also applied the extrapolation scheme based on the h dependence on $N\sigma^{1/2}$ (derived in our work) to calculate the heights of PEO brushes using N and σ taken from the fully atomistic molecular dynamics simulations pertaining to PEO chains densely attached at the graphite surface carried out by Bedrov and Smith.[30] Such extrapolated heights are systematically lower by about 20% than those calculated in their work. Similar comparisons with another coarse-grained molecular dynamics study of polar polymer brushes in good polar solvent which might be mapped to hydrated PEO brushes[67] yields lower extrapolated heights as well.

4. CONCLUSIONS

The monomer density distribution functions of PEO chains chemically attached by one terminal atom to the siloxane surface exhibit fine structuring near the solid surface peculiar for the atomistic systems and quite different from the SCF predictions. Positions of the initial oscillations in the EO monomer density distribution functions remain essentially unchanged upon hydration but their amplitudes are diminished when compared with the dry analogues and only the first three peaks are preserved in water. The disagreement between the probability distribution of the free chain ends achieved from MD simulations and the SCF theory is even deeper. These discrepancies are attributed to the short PEO chain lengths and specific interactions between components in the investigated systems which do not fulfill the requirements defining the model systems subject to the SCF analysis.

The chains adopt a mushroom conformation at the coverage densities which disable their mutual overlap. The potential two-dimensional pancake-like entities in the nonoverlapping regime, adsorbed on the siloxane surface, were ruled out by scaling of the chain dimensions with the contour chain length and by the reduced intensities of amplitudes of the monomer density distributions of hydrated layers when compared with the analogous amplitudes for adsorbing dry PEO layers. From the dependence of h/N vs σ, we were able to estimate the brush regime for chains of $N = 24$ and 30 monomers at the coverage densities $\sigma \geq 0.437\ \mathrm{nm}^{-2}$. For chains of $N = 18$ monomers, this coverage density is at about the onset of the brush regime. The coverage densities at which the brush regime exists are for all chain lengths larger than $1/(\pi R_g^2)$ in accordance with the assumed onset.

Although, the Flory interaction parameter classifies water as a good solvent for PEO polymers, the average height of the investigated brushes follows $N\sigma^{1/2}$ (typical for the Θ solvents) instead of the $N\sigma^{1/3}$ dependence. This evolution virtually corresponds to the concentrated solution with the correlation length scale equal to the distance between grafting points and smaller than the thermal blob size. Moreover, even the free investigated chains are too short to adopt configurations corresponding to good-solvent conditions. The heights of the brush layers reproduce fairly well the experimental figures, which for PEO chain lengths and the conditions frequently employed in experiments on brush systems, are also highly probable to conform to the concentrated-solution regime.

AUTHOR INFORMATION

Corresponding Author
*E-mail upolzben@savba.sk.

ACKNOWLEDGMENT

This work was supported by a postdoc FCT Grant SFRH/BPD/63568/2009 with financial support from European Social Found, REQUIMTE, the Science and Technology Assistance Agency under the contract No. APVV-0079-07 and by VEGA Grant 2/0144/09, and in part by the Centre of Excellence Program of the Slovak Academy of Sciences (COMCHEM).

REFERENCES

(1) Klein, J. *Annu. Rev. Mater. Sci.* **1996**, *26*, 581–612.
(2) Napper, D. H. *Polymeric Stabilization of Colloidal Dispersions*; Academic Press: London, 1983.
(3) Amiji, M.; Park, K. *J. Biomater. Sci. Polym. Ed.* **1993**, *4*, 217–234.
(4) Szleifer, I.; Carignano, M. A. *Macromol. Rapid Commun.* **1999**, *21*, 423–448.
(5) Lasic, D. D.; Papahadjopoulos, D. *Curr. Opin. Solid State Mater. Sci.* **1996**, *1*, 392–400.
(6) Szleifer, I. *Curr. Opin. Solid State Mater. Sci.* **1997**, *2*, 337–344.
(7) Lee, S.-W.; Laibinis, P. E. *Biomaterials* **1998**, *19*, 1669–1675.
(8) Mathe, G.; Gege, C.; Neumaier, K. R.; Schmidt, R. R.; Sackmann, E. *Langmuir* **2000**, *16*, 3835–3845.
(9) Alexander, S. *J. Phys. (Paris)* **1977**, *38*, 983–987.
(10) de Gennes, P.-G. *Macromolecules* **1980**, *13*, 1069–1075.
(11) Milner, S. T.; Witten, T. A.; Cates, M. E. *Europhys. Lett.* **1988**, *5*, 413–418.
(12) Milner, S. T.; Witten, T. A.; Cates, M. E. *Macromolecules* **1988**, *21*, 2610–2619.
(13) Milner, S. T. *Science* **1991**, *251*, 905–914.
(14) Muthukumar, M.; Ho, J.-S. *Macromolecules* **1989**, *22*, 965–973.
(15) Seidel, C.; Netz, R. R. *Macromolecules* **2000**, *33*, 634–640.
(16) Carignano, M. A.; Szleifer, I. *J. Chem. Phys.* **1993**, *98*, 5006–5018.
(17) Carignano, M. A.; Szleifer, I. *Macromolecules* **1995**, *28*, 3197–3204.
(18) Watanabe, H.; Tirroll, M. *Macromolecules* **1993**, *26*, 6455–6466.
(19) Auroy, P.; Auvray, L.; Leger, L. *Macromolecules* **1991**, *24*, 2523–2528.
(20) Kent, M. S. *Macromol. Rapid Commun.* **2000**, *21*, 243–270.
(21) Grest, G. S.; Murat, M. *Macromolecules* **1989**, *22*, 4054–4059.
(22) Grest, G. S.; Murat, M. *Macromolecules* **1993**, *26*, 3108–3117.
(23) Grest, G. S. *Macromolecules* **1994**, *27*, 418–426.
(24) Chakrabarti, A.; Toral, R. *Macromolecules* **1990**, *23*, 2016–2021.
(25) Lai, P.-Y.; Binder, K. *J. Chem. Phys.* **1991**, *95*, 9288–9299.
(26) Chakrabarti, A. *J. Chem. Phys.* **1994**, *100*, 631–635.
(27) Karaiskos, E.; Bitsanis, I. A.; Anastasiadis, S. H. *J. Polym. Sci., Part B: Polym. Phys.* **2009**, *47*, 2449–2461.
(28) Pal, S.; Seidel, C. *Macromol. Theory Simul.* **2006**, *15*, 668–673.
(29) Binder, K.; Neelov, I. M. *Macromol. Theory Simul.* **1995**, *4*, 119–136.
(30) Bedrov, D.; Smith, G. D. *Langmuir* **2006**, *22*, 6189–6194.
(31) Träskelin, P.; Kuhl, T. L.; Faller, R. *Phys. Chem. Chem. Phys.* **2009**, *11*, 11324–11332.
(32) Li, T.; Park, K. *Comput. Theor. Polymer. Sci.* **2001**, *11*, 133–142.
(33) Duque, D.; Peterson, B. K.; Vega, L. F. *J. Phys. Chem. C* **2010**, *111*, 12328–12334.
(34) Elbert, D. L.; Hubbell, J. A. *Annu. Rev. Mater. Sci.* **1996**, *26*, 365–394.
(35) Murthy, R.; Bailley, B. M.; Valentin-Rodriguez, C.; Ivanisevic, A.; Grunlan, M. A. *J. Polym. Sci., Part A: Polym. Chem.* **2010**, *48*, 4108–4119.
(36) Dormidontova, E. E. *Macromolecules* **2002**, *35*, 987–1001.
(37) Kjellander, R.; Florin, E. *J. Chem. Soc., Faraday Trans. 1* **1981**, *77*, 2073–2077.
(38) Walkenhorst, R.; Selser, J. C.; Piet, G. *J. Chem. Phys.* **1998**, *109*, 11043–11050.
(39) van der Spoel, D.; Lindahl, E.; Hess, B.; Groenhof, G.; Mark, A. E.; Berendsen, H. J. C. *J. Comput. Chem.* **2005**, *26*, 1701–1719.
(40) Hess, B.; van der Spoel, D.; Lindahl, E. *J. Chem. Theory Comput.* **2008**, *4*, 435–447.
(41) Vorobyov, I.; Anisimov, V. M.; Green, S.; Venable, R. M.; Moser, A.; Pastor, R. W.; MacKerell, A. D. *J. Chem. Theory Comput.* **2007**, *3*, 1120–1133.
(42) Lee, H.; Venable, R. M.; MacKerell, D. J.; Pastor, R. W. *Biophys. J.* **2008**, *95*, 1590–1599.
(43) Jorgensen, W. L.; Chandrasekhar, J.; Madura, J. D. *J. Chem. Phys.* **1983**, *79*, 926–935.
(44) Mark, P.; Nilsson, L. *J. Comput. Chem.* **2002**, *23*, 1211–1219.
(45) Bjelkmar, P.; Larsson, P.; Cuendet, M. A.; Hess, B.; Lindahl, E. *J. Chem. Theory Comput.* **2010**, *6*, 459–466.
(46) Cruz-Chu, E. R.; Aksimentiev, A.; Schulten, K. *J. Phys. Chem. B* **2006**, *110*, 21497–21508.

(47) Manuscript in preparation
(48) Parrinello, M.; Rahman, A. *J. Appl. Phys.* **1981**, *52*, 7182–7190.
(49) Nosé, S.; Klein, M. L. *Mol. Phys.* **1983**, *50*, 1055–1076.
(50) Hess, B. *J. Chem. Theory Comput.* **2007**, *4*, 116–122.
(51) Nosé, S. *Mol. Phys.* **1984**, *52*, 255–268.
(52) Hoover, W. G. *Phys. Rev. A* **1985**, *31*, 1695–1697.
(53) Darden, T.; York, D.; Pedersen, L. *J. Chem. Phys.* **1993**, *98*, 10089–10092.
(54) Essmann, U.; Perera, L.; Berkowitz, M. L.; Darden, T.; Lee, H.; Pedersen, L. *J. Chem. Phys.* **1995**, *103*, 8577–8592.
(55) Manuscript in preparation
(56) Rubinstein, M.; Colby, R. H. *Polymer Physics*, 1st ed.; Oxford University: New York, 2003.
(57) Lee, J. H.; Lee, H. B.; Andrade, J. D. *Prog. Polym. Sci.* **1995**, *20*, 1043–1079.
(58) Yamakawa, H. *Modern Theory of Polymer Solution*; Harper & Row Publishers: New York, 1971.
(59) Roosjen, A.; van der Mei, H. C.; Busscher, H. J.; Norde, W. *Langmuir* **2004**, *20*, 10949–10955.
(60) Mark, J. E.; Flory, P. J. *J. Am. Chem. Soc.* **1965**, *87*, 1415–1423.
(61) Eliassi, A.; Modarress, H.; Monsoori, G. A. *J. Chem. Eng. Data* **1999**, *44*, 52–55.
(62) Utz, M.; Begley, M. R. *J. Mech. Phys. Solids* **2008**, *56*, 801–814.
(63) Özdemir, C.; Güner, A. *J. Appl. Polym. Sci.* **2006**, *101*, 203–216.
(64) Piehler, J.; Brecht, A.; Valiokas, R.; Liedberg, B.; Gauglitz, G. *Biosens. Bioelectron.* **2000**, *15*, 473–481.
(65) Kuhl, T. L.; Majewski, J.; Wong, J. Y.; Steinberg, S.; Leckband, D. E.; Israelachvili, J. N.; Smith, G. S. *Biophys. J.* **1998**, *75*, 2352–2362.
(66) McNamee, C. E.; Yamamoto, S.; Higashitani, K. *Langmuir* **2007**, *23*, 4389–4399.
(67) Elliott, I. G.; Kuhl, T. L.; Faller, R. *Macromolecules* **2010**, *43*, 9131–9138.